

1 Simulation of the time resolution of a 50 μm low-gain
2 avalanche detector.

3 C. Peña^{*,a,b}, G. Deptuch^a, S. Xie^b, A. Apresyan^a, L. Narvaez^b, T. Liu^a, N. Cartiglia^c

4 ^a*Fermi National Accelerator Laboratory, Batavia, IL, USA*

5 ^b*California Institute of Technology, Pasadena, CA, USA*

6 ^c*INFN, Torino, Italy*

7 **Abstract**

In this paper we report simulation results on the timing resolution of a 50 μm low-gain avalanche detector (LGAD). The simulation includes: sensor fluctuations, front-end electronics, and quantization. Comparisons on the performance for different front-end electronics (FEE) bandwidths (BW) are presented, as well as the dependance on singal-to-noise ratio (SNR). Two approaches to measure the timestamp are considered: leading edge (LE) and constant fraction (CF). Additionally, the time resolution is studied as function of the irradiation of the sensor. Simulated LGAD pulses before irradiation, and after neutron fluences of $5 \times 10^{14} \text{ n/cm}^2$ and $1 \times 10^{15} \text{ n/cm}^2$, are studied. The time resolution a 50 μm LGADs was found to be 35 ps for FE electronics BWs larger than 350 MHz and SNRs larger than 30. The time resolution at a SNR of 30 for fluences of $5 \times 10^{14} \text{ n/cm}^2$ and $1 \times 10^{15} \text{ n/cm}^2$ were found to be 31 ps and 37 ps, respectively.

8 *Key words:*

9 Silicon, Timing, LGAD

10 **Contents**

11	1 Introduction	2
12	2 Simulation Framework	2
13	2.1 Fron-end electronics and noise injection	3
14	2.1.1 front-end implementation	3
15	2.1.2 noise injection	4
16	3 Timing Reconstruction and Analysis	4
17	3.1 Leading edge and constant fraction discriminators	5
18	3.2 Time-walk correction and time-over-threshold	5

*Corresponding author

Email address: cmorgoth@fnal.gov (C. Peña)

19	4 LGAD Front-end Electronics Performance	7
20	4.1 Front-end electronics shaping time and SNR studies	7
21	4.2 Timing Performace as a function of irradiation	9
22	5 Conclusion	9

1. Introduction

LGADs are envisioned to be used in the CMS and ATLAS experiment upgrades for HL-LHC in order to overcome the event reconstruction challenges posed by the high rate of concurrent collisions per beam crossing. The implemented regions of pseudorapidity (η) are: $|\eta| > 1.5$, and $2.4 < |\eta| < 4.2$ for CMS and ATLAS, respectively. In order to achieve the desired timing precision across a large area of the detectors, the sensors will need to provide high uniformity of signal response and timing resolution. Beam test measurements have provided encouraging results towards achieving such detectors [1].

In this paper, we report simulation results on the timing resolution of a $50\ \mu\text{m}$ low-gain avalanche detector (LGAD) which includes the effects of the sensor fluctuations, front-end electronics (FEE), and quantization. Our results indicate that for FEE analog bandwidths (BW) larger than 350 MHz (shaping times $< 1\ \text{ns}$) and signal-to-noise ratios (SNRs) larger than 30, time resolutions of $30 - 37\ \text{ps}$ and $34 - 47\ \text{ps}$ are obtained when using constant fraction (CF) and leading edge (LE) discriminators, respectively. These results are compatible with previous measurements on LGAD timing resolutions carried out in laboratory and beam test conditions [1–3]. We study the time resolution of four different FEE shaping times: 0.5 ps, 1.0 ps, 2.0 ps, and 4.0 ps; three SNR: 20, 30, 100; and three irradiation levels: pre-radiation, $5 \times 10^{14}\ \text{n/cm}^2$, and $1 \times 10^{15}\ \text{n/cm}^2$. For every point in this scan we evaluate the time resolution for LE and CFD.

The paper is organized as follows: the simulation is described in Sec. 2; algorithms used in the timing reconstruction and analysis are described in Sec. 3; simulation results are presented in Sec. 4, followed by the conclusion in Sec. 5.

2. Simulation Framework

The simulation framework is based on c++ programming language. The LGAD pulses are obtained from Weightfield2 (WF2), a 2-dimensional silicon simulator [4]. WF2 provides sets of 1000 LGAD pulses which models the response of the sensor to minimum ionizing particles (MIPs). We generated 3 sets of LGAD pulses for a $50\ \mu\text{m}$ LGAD: pre-irradiation, and after neutron fluences of $5 \times 10^{14}\ \text{n/cm}^2$ and $1 \times 10^{15}\ \text{n/cm}^2$. The simulation framework takes the LGAD pulses (from WF2) and adds gaussian white noise (hereafter white noise). At this point the LGAD pulses with the added white noise are fed into the simulation of the FEE (see Fig. 1). The output of the FEE simulation is the convolution of the impulse response function and the input signal at the FEE. We consider four shaping constants for the impulse response of the FEE: 0.5, 1.0, 2.0, and 4.0 ns (the FEE simulation is described in Sec. 2.1). At the output of the FEE block we have a simulated LGAD pulse which includes the effects of sensor fluctuations, shaping of the FEE, and noise. A waveform analysis is performed with the pulses obtained at the output of the FEE block. We assign timestamps to each pulse by using algorithms that

emulate an ideal LE and CF discriminators. For each threshold we obtain a LE and CF timestamp as well as the corresponding time-over-threshold (ToT) of the pulse. The SNR is defined as the ratio of the most probable value (MPV) of the amplitude distribution to the width of the amplitude distribution at a fixed sample (where only noise is present). We study 3 SNR scenarios: 20, 30, and 100. A schematic diagram of the simulation is shown in Fig. 1.

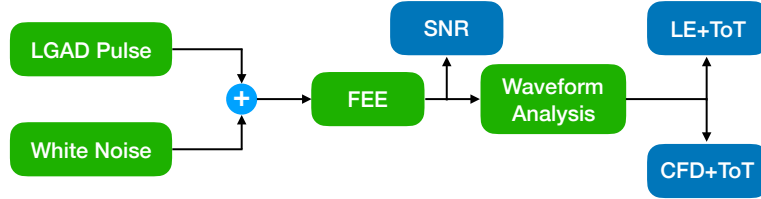


Figure 1: A schematic diagram of the simulation. Each simulation configurable block is shown in green. The most relevant outputs of the simulation are shown in blue.

2.1. Fron-end electronics and noise injection

The front-end simulation is implemented in c++ programing language. It combines analytical calculations when possible but it mostly relies on numerical methods. We implement most calculations in the time domain, while the frequency domain is mostly used to cross-check noise and the FEE expected responses. Sections 2.1.1 and 2.1.2 detail the front-end and noise implementation in the simulation.

2.1.1. front-end implementation

The fron-end simulation is based on a single amplification stage. We focus on the BW of such amplifier rather than variations thereof. The FEE is a second order low-pass filter which transfer function and impulse response are given by equations 1 and 2, respectively.

$$H(S) = \frac{\frac{1}{\tau_s^2}}{(S + 1/\tau_s)^2} \quad (1) \quad h(t) = \frac{t}{\tau_s^2} e^{-t/\tau_s} \quad (2)$$

The output pulse of the FEE is the convolution (in time domain) of the pulse from the LGAD library and the FEE impulse response (see Eq. 2). The time base for the pulses and the convolution is 10 ps – this sampling time is used throughout the simulation. As stated above we focus the study on the BW of the FEE, to that end we scan the τ_s paremeter in Eq. 2 in the following set: {0.5, 1, 2, 4} ns, this parameter is hereafter referred to as shaping time (ST). Figure 2 (left) shows the comparison of the impulse and LGAD responses for a ST of 1 ns while Figure 2 (right) shows the LGAD response for all STs studied. We observe that the LGAD response is delayed with respect to the impulse response, and that pulse slew rate is decreased in the first nanosecond of the pulse. We also observe the expected behavior when comparing the LGAD responses for the different STs, pulse risetimes scale with the ST and the decay time is dominated by the ST. The measured 10 - 90% risetimes are shown in Tab. 1.

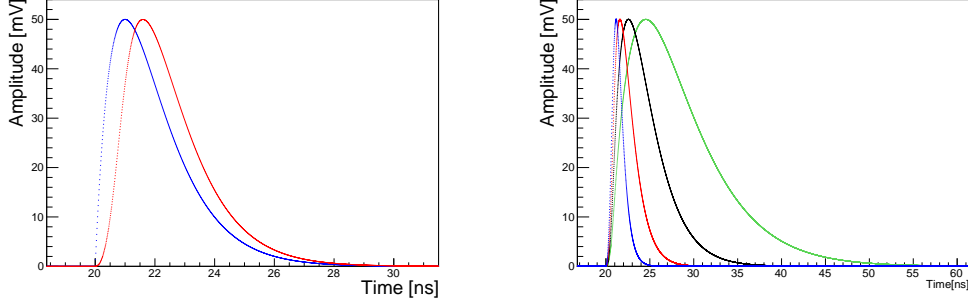


Figure 2: (Left) Comparison of impulse and LGAD responses for the a shaping time (ST) of 1 ns. (Right) LGAD response for the four shaping times studied: $\{0.5, 1, 2, 4\}$ ns. All pulses have been normalized to achieve a peak amplitude of 50 mV. Legends for the shaping times are shown in the plots.

Shaping time (ns)	0.5	1.0	2.0	4.0
Risetime (ns)	$0.7 \pm xx$	$0.9 \pm xx$	$1.4 \pm xx$	$2.5 \pm xx$

Table 1: Measured risetime for all shaping times studied: $\{0.5, 1, 2, 4\}$ ns. Risetime is the 10% – 90% time difference as measured by the CFD algorithm described in Sec. 3.1.

2.1.2. noise injection

Gaussian white noise is simulated by sampling the full time window (0 - 100 ns) in 10 ps intervals. Each sampled time is assign a random amplitude which is drawn from from a gaussian distribution with zero mean and width corresponding to the SNR under study. It is important to note that the width of the gaussian parameter is not exactly the SNR and needs to be adjusted depending on the ST of the FEE. The left panel of Figure 3 shows the gaussian white noise before and after a 1 ns FEE. The expected behavior for the noise is observed. The left panel of Figure 3 shows the output of the FEE block, with a 1 ns ST, for a pre-radiation LGAD pulse when noise has been injected. The injected noise is such that the SNR is 30. SNR is defined ratio of the landau peak of the maximum amplitude (MPV) to the the r.m.s of the 100th sample over an ensemble of 1000 pulses.

3. Timing Reconstruction and Analysis

The time reconstruction is based on a waveform analysis. We generate an ensemble of 1000 pulses sampled every 10 ps. Each pulse is interpolated using a the Whittaker-Shannon formula $(\sin(x)/x)$, using the interpolated pulse we assign a timestamp by finding when each pulse crosses a voltage threshold. The threshold can be a constant value (LE) or a constant fraction of the maximum amplitude of pulse (CFD), more details about the algorithms are given in Sec. 3.1. The time resolution is estimated by the width parameter of a gaussian fit to the timestamps obtain for a particular threshold. We apply a time time-walk correction based on the time-over-threshold of the pulse, we note that this correction has a large improvement on the time resolution measured using the LE algorithm while the CFD algorithm is mostly insentive to this correction. Details about

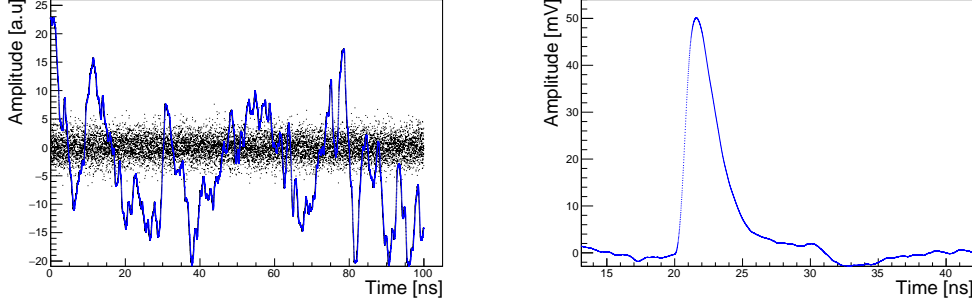


Figure 3: (Left) Comparison of gaussian white noise before and after the FEE. (Right) Example pulse at the output of the FEE block with a SNR of 30. Both figure use a shaping time (ST) of 1 ns. Legends for the shaping times are shown in the plots.

113 this correction are covered in Sec. 3.2. The timestamps are measured with a 20 ps bin-
 114 ning while the time-over-threshold is measured with a 100 ps in order to simulate the
 115 effect of quantization. We scan the LE and CFD threshold such that we find the one
 116 with the lowest jitter.

117 3.1. Leading edge and constant fraction discriminators

118 The leading edge and constant fraction discriminator algorithms are ideal in the sense
 119 that they don't simulate the effect of electronics in a real implementation. The approach
 120 taken is to sample the pulses every 10 ps and subsequently interpolate them using a the
 121 WhittakerShannon formula ($\sin(x)/x$) to more accurately find the threshold crossing.
 122 In the LE case the threshold is scanned from 3 - 60 mV, while the CFD is scanned
 123 from 5 - 90 % of the current pulse maximum amplitude. For each threshold we obtain
 124 two timestamps: when the pulse first crosses the threshold (t_0) and when it crosses the
 125 second time (t_1), now in the opposite direction. The time-over-threshold is defined as
 126 the difference of the two timestamps ($\text{ToT} = t_1 - t_0$). The first timestamp, t_0 , is used
 127 to determine the time resolution at given threshold. The time resolution is defined as
 128 the width of a gaussian fit to the t_0 distribution binned with a bin-width of 20 ps. The
 129 time resolution is obtained in two cases: before and after a time-walk correction. The
 130 time-walk correction aims to correct the known drift effect on the timestamps when
 131 dealing with pulses of different amplitudes. The time walk correction is based on the
 132 measured ToT and explained in detail in Sec. 3.2. We note that the effect of the time-
 133 walk correction is large for LE and almost negligible for CFD. Fig. 4 shows a typical t_0
 134 distribution, using the LE and CFD algorithms, for the pre-radiation LGAD after the
 135 ToT correction has been applied. The time resolution (σ_t) is measured to be 37.6 ± 2.0
 136 and 32.9 ± 1.4 for the LE and CFS, respectively.

137 3.2. Time-walk correction and time-over-threshold

138 A time-walk correction is applied in order to correct the timestamp drift when dealing
 139 with pulse of varying amplitudes. The correction is based on the measured time-over-
 140 threshold: $\text{ToT} = t_1 - t_0$. We observe, as expected, that ToT correction is large for the LE
 141 case and negligible for CFD (see Fig. 6). Figure (left) 5 show a typical two dimensional

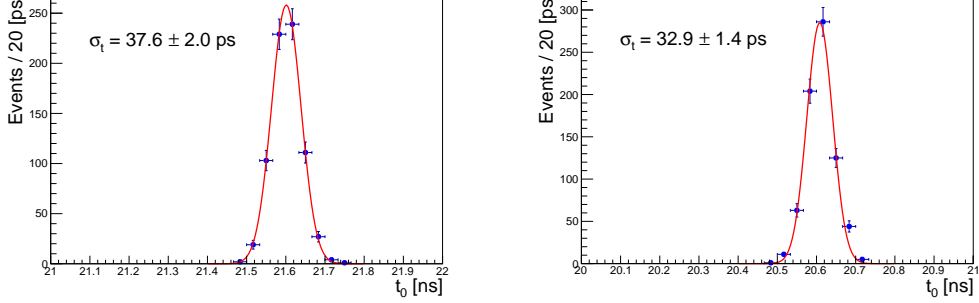


Figure 4: (Left) timestamp (t_0) distribution for a 30 mV threshold using a leading edge discriminator. (Left) timestamp (t_0) distribution for a 35% threshold using a constant fraction discriminator. Both figures include the time-walk correction based on the measured ToT. Both figures use a shaping time (ST) of 1 ns and correspond to SNR of 30.

map of t_0 and ToT for the LE algorithm, wherein a clear correlation between t_0 and ToT is observed. The time-walk correction is obtain by measuring the average t_0 in each ToT bin and subsequently fitting a 2th-order polinomial (see Fig. (right) 5). The resulting analytical expression after the fit is then used to correct the dependece of t_0 on ToT. The time-walk correction is expressed in Eq. 3, where p_2 and p_1 are the quadratic and linear coefficients of the 2th-oder polinomial fit. The procedure is updated every time any parameter on the simulation changes, i.e ST, SNR, and LGAD library inputs. As shown in Fig. (left) 6 the effect of the time-walk depends on the threshold used and correcting for it can yield significant improvements in the time resolution.

$$t_0 = t_0 - (p_2 \text{ToT}^2 + p_1 \text{ToT}) \quad (3)$$

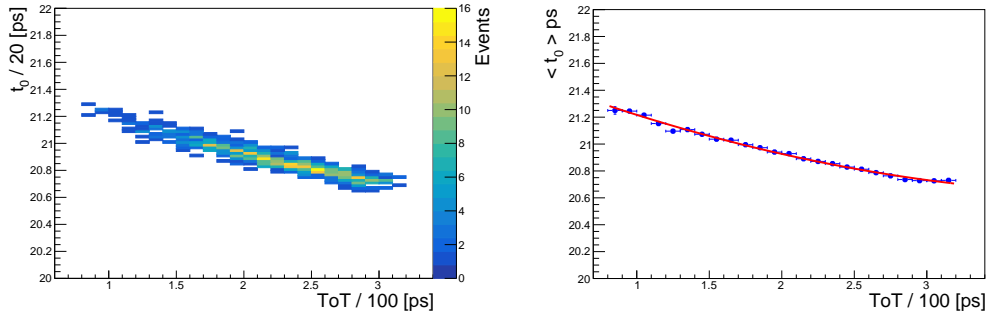


Figure 5: (Left) two dimensional map of the timestamp (t_0) and ToT ($t_1 - t_0$). (Right) one dimensional projection of the timestamp (t_0) dependence on ToT, the red curve is the 2th-order polinomial fit that ultimately is used to correct t_0 . Both figures use a shaping time (ST) of 1 ns and correspond to a SNR of 30.

4. LGAD Front-end Electronics Performance

Herein we present a number of studies for different a 50 μm LGAD. We study the time resolution as a function of irradiation for three different scenarios: pre-radiation, and after neutron fluences of $5 \times 10^{14} \text{ n/cm}^2$ and $1 \times 10^{15} \text{ n/cm}^2$. We also quantify the effect of the BW of the FEE by varying the the ST (τ_s), four STs are considered: $\{0.5, 1, 2, 4\}$ ns. Additionally, we study the effect of noise by varying the SNR in all the scenarios described above. We consider three SNR: 20, 30, and 100. Sec. 4.1 summarizes the effect of the shaping time, Sec. summarizes the effect of SNR, and and Sec. 4.2 summarizes the effect of LGAD radiation.

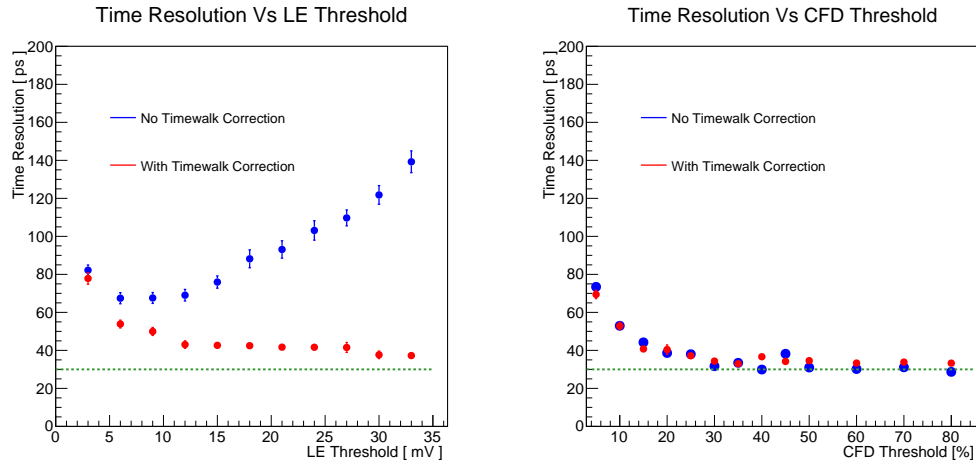


Figure 6: (Left) Comparison of gaussian white noise before and after the FEE. (Right) Example pulse at the output of the FEE block with a SNR of 30. Both figure use a shaping time (ST) of 1 ns. Legends for the shaping times are shown in the plots.

4.1. Front-end electronics shaping time and SNR studies

We scan the ST of the FEE and the SNR. The results for the pre-radiation sensor are summarized in Table. 4.1. We observe that the best results are consistently obtained by the 0.5 and 1.0 ns STs regardless of the SNR. We also observe that longer STs are more affected by less favorable SNR, e.g for and SNR of 20 the time resolution is 37 ps and 100 ps for a 0.5 ns and 4.0 ns ST, respectively. We also observe that CFD consistently outperforms LE, this effect is more clearly observed for less favorable SNR and slower ST. Comparing CFD and LE for the 1.0 ns ST with SNR of 20 yields a difference in performance of 35 ps (when subtrated in quadrature). Additionally, we observe that time resolution better than 25 ps could not be achieved which is consistent with the known intrinsic LGAD jitter. This last effect is taken into account by the WF2 pulse library and confirmed in our simulation where we use a SNR of 1000 and obtained a time resolution consistent with 25 ps. Finally, in the case of the pre-radiation sensor we observed that time resolutions of the order of 30 - 35 ps are achievable for STs between 0.5 - 1.0 ns and a SNR of 30.

ST (ns)	Time Resolution (ps)					
	Leading Edge			Constant Fraction		
	SNR = 20	SNR = 30	SNR = 100	SNR = 20	SNR = 30	SNR = 100
0.5	38.4 ± 2.1	34.9 ± 1.7	28.8 ± 1.0	37.2 ± 1.9	34.5 ± 1.6	29.8 ± 1.9
1.0	45.4 ± 2.2	37.3 ± 1.4	28.7 ± 1.7	36.4 ± 1.8	33.0 ± 1.4	25.9 ± 1.3
2.0	63.4 ± 2.5	47.6 ± 2.0	30.7 ± 1.2	47.6 ± 1.9	34.3 ± 1.6	28.7 ± 1.7
4.0	103.0 ± 4.1	75.3 ± 2.8	37.6 ± 2.0	73.8 ± 3.1	54.8 ± 2.1	32.1 ± 1.3

Table 2: 50 μm pre-radiation LGAD sensor simulation: summary of best time resolution obtained for SNRs of 20, 30, and 100. Leading edge and constant fraction results are shown.

ST (ns)	Time Resolution (ps)					
	Leading Edge			Constant Fraction		
	SNR = 20	SNR = 30	SNR = 100	SNR = 20	SNR = 30	SNR = 100
0.5	36.8 ± 1.9	32.0 ± 1.3	26.0 ± 1.2	32.5 ± 1.4	30.6 ± 1.2	25.1 ± 1.2
1.0	40.9 ± 1.4	33.8 ± 1.1	29.2 ± 1.0	33.4 ± 1.5	30.9 ± 0.9	26.1 ± 1.3
2.0	56.9 ± 2.4	45.3 ± 2.2	30.1 ± 1.1	43.7 ± 1.6	36.9 ± 1.3	24.4 ± 1.0
4.0	93.3 ± 3.6	67.9 ± 2.5	36.5 ± 1.3	70.8 ± 2.8	52.4 ± 1.9	29.9 ± 1.9

Table 3: 50 μm LGAD sensor simulation after neutron fluence of 5×10^{14} n/cm²: summary of best time resolution obtained for SNRs of 20, 30, and 100. Leading edge and constant fraction results are shown.

ST (ns)	Time Resolution (ps)					
	Leading Edge			Constant Fraction		
	SNR = 20	SNR = 30	SNR = 100	SNR = 20	SNR = 30	SNR = 100
0.5	47.8 ± 2.0	37.6 ± 2.0	26.6 ± 1.3	41.9 ± 1.9	34.3 ± 1.1	24.1 ± 1.0
1.0	59.9 ± 2.3	46.8 ± 1.8	28.1 ± 1.5	46.5 ± 1.9	36.8 ± 1.3	23.1 ± 0.9
2.0	89.7 ± 3.5	68.2 ± 2.6	32.3 ± 1.4	64.7 ± 2.8	49.6 ± 2.1	27.3 ± 0.9
4.0	147.3 ± 5.1	109.0 ± 4.3	42.6 ± 1.9	118.6 ± 4.0	84.1 ± 3.2	33.8 ± 1.1

Table 4: 50 μm LGAD sensor simulation after neutron fluence of 1×10^{15} n/cm²: summary of best time resolution obtained for SNRs of 20, 30, and 100. Leading edge and constant fraction results are shown.

4.2. Timing Performace as a function of irradiation

We study the effect of irradiation on the time resolution of a 50 μm sensor, we employ LGAD simulation files that include the effect of radiation damage. We consider two cases besides pre-radiation: neutron fluences of $5 \times 10^{14} \text{ n/cm}^2$ and $1 \times 10^{15} \text{ n/cm}^2$. We perform the same studies as in the pre-radiation case and covered in Sec. 4.1. The results for the irradiated LGAD are presented in Table ?? and Table 4.1 for neutron fluences of $5 \times 10^{14} \text{ n/cm}^2$ and $1 \times 10^{15} \text{ n/cm}^2$, respectively. The ratios of the simulated sensor were 3:3:2 for the pre-radiation, $5 \times 10^{14} \text{ n/cm}^2$, and $1 \times 10^{15} \text{ n/cm}^2$. The observe similar trends to those of the pre-radiation sensor described in Sec. 4.1. We note that when using STs between 0.5 - 1.0 ns and a SNR of 30, time resolutions of the order of 30 - 35 ps and 40 - 50 ps are obtained for $5 \times 10^{14} \text{ n/cm}^2$ and $1 \times 10^{15} \text{ n/cm}^2$, respectively.

5. Conclusion

We study the time resolution of a 50 μm LGAD under using a simulation. We focus on the shaping time and sigal-to-noise ratio of the fron-end electronics and its interplay with the irradiation of the sensor. We reproduce the known LGAD jitter of 25ps for fast STs and large SNRs. We observe a clear degradation of the time resolution with SNR and slower STs. The best results are obtained using a ST of 0.5 ns and using CFD – similar results are obtained with a ST of 1.0 ns. For a SNR of 30 and for STs between 0.5-1.0 ns we obtain time resoutions between 30-37 ps for the 3 irradiations considered. The reduction in gain with irradiation could bring the SNR for the most irradiated LGAD ($1 \times 10^{15} \text{ n/cm}^2$) to 20 and thus worsen the time resolution to 42-47 ps. We also observe a clear edge of performace of CF over LE discriminators, particularly at low SNR and largest irradiation level. For the 1.0 ns at SNR = 30, the performance improvement of CF over LE is 26ps for the pre-radiation sensor while 37ps for $1 \times 10^{15} \text{ n/cm}^2$. Overall our simulation results indicate that time resolutions i 45 ps are accesible for a 50 μm LGADs up to irradiations of $1 \times 10^{15} \text{ n/cm}^2$.

Acknowledgment

We thank the FTBF personnel and Fermilab accelerator’s team for very good beam conditions during our test beam time. We also appreciate the technical support of the Fermilab SiDet department for the rapid production of wire-bonded and packaged LGAD assemblies. We would like to thank Alan Prosser and Ryan Rivera for their critical help in setting up the DAQ and trigger chain. We thank Ned Spencer, Max Wilder, and Forest McKinney-Martinez for their technical assistance, and the CNM and HPK manufacturing team. We acknowledge the help of V. Cindro and I. Mandic with the neutron irradiations.

This document was prepared using the resources of the Fermi National Accelerator Laboratory (Fermilab), a U.S. Department of Energy, Office of Science, HEP User Facility. Fermilab is managed by Fermi Research Alliance, LLC (FRA), acting under Contract No. DE-AC02-07CH11359. Part of this work was performed within the framework of the CERN RD50 collaboration.

This work was supported by the Fermilab LDRD 2017.027; by the United States Department of Energy grant DE-FG02-04ER41286; by the California Institute of Technology High Energy Physics under Contract DE-SC0011925; by the European Union’s

217 Horizon 2020 Research and Innovation funding program, under Grant Agreement no.
 218 654168 (AIDA-2020) and Grant Agreement no. 669529 (ERC UFSD669529); by the
 219 Italian Ministero degli Affari Esteri and INFN Gruppo V; and by the Spanish Min-
 220 istry of Economy, Industry and Competitiveness through the Particle Physics National
 221 Program (ref. FPA2014-55295-C3-2-R and FPA2015-69260-C3-3-R) co-financed with
 222 FEDER funds.

223 References

- 224 [1] A. Apresyan, S. Xie, C. Pena, *et al.*, “Studies of Uniformity of 50 μm Low-Gain Avalanche Detectors
 225 at the Fermilab Test Beam,” *Nucl. Instrum. Meth.*, vol. A895, pp. 158–172, 2018.
- 226 [2] N. Cartiglia *et al.*, “Beam test results of a 16 ps timing system based on ultra-fast silicon detectors,”
 227 *Nucl. Instrum. Meth. A*, vol. 850, pp. 83 – 88, 2017.
- 228 [3] G. Pellegrini, P. Fernández-Martínez, M. Baselga, C. Fleta, D. Flores, V. Greco, S. Hidalgo,
 229 I. Mandić, G. Kramberger, D. Quirion, and M. Ullan, “Technology developments and first mea-
 230 surements of Low Gain Avalanche Detectors (LGAD) for high energy physics applications,” *Nuclear*
 231 *Instruments and Methods in Physics Research Section A: Accelerators, Spectrometers, Detectors*
 232 *and Associated Equipment*, vol. 765, pp. 12 – 16, 2014. HSTD-9 2013 - Proceedings of the 9th
 233 International.
- 234 [4] H. F. W. Sadrozinski, A. Seiden, and N. Cartiglia, “4D tracking with ultra-fast silicon detectors,”
 235 *Rept. Prog. Phys.*, vol. 81, no. 2, p. 026101, 2018.